nature communications

Article

https://doi.org/10.1038/s41467-024-53027-5

Foot-and-mouth disease virus antigenic landscape and reduced immunogenicity elucidated in atomic detail

Received: 21 February 2024

Accepted: 24 September 2024

Published online: 10 October 2024

Check for updates

Haozhou Li[1,5], Pan Liu[2,3,5], Hu Dong[1,5], Aldo Dekker[4], Michiel M. Harmsen[4], Huichen Guo[1,6] ✉, Xiangxi Wang[2,6] ✉ & Shiqi Sun[1,6] ✉

Unlike most other picornaviruses, foot-and-mouth disease (FMD) intact virions (146S) dissociate easily into small pentameric subunits (12S). This causes a dramatically decreased immunogenicity by a mechanism that remains elusive. Here, we present the high-resolution structures of 12S (3.2 Å) and its immune complex of a single-domain antibody (VHH) targeting the particle interior (3.2 Å), as well as two 146S-specific VHHs complexed to distinct sites on the 146S capsid surface (3.6 Å and 2.9 Å). The antigenic landscape of 146S is depicted using 13 known FMD virus-antibody complexes. Comparison of the immunogenicity of 146S and 12S in pigs, focusing on the resulting antigenic sites and incorporating structural analysis, reveals that dissociation of 146S leads to structural alteration and destruction of multiple epitopes, resulting in significant differences in antibody profiles/lineages induced by 12S and 146S. Furthermore, 146S generates higher synergistic neutralizing antibody titers compared to 12S, whereas both particles induce similar total FMD virus specific antibody titers. This study can guide the structure-based rational design of novel multivalent and broad-spectrum recombinant vaccines for protection against FMD.

Foot-and-mouth disease (FMD), a highly relevant infectious disease of cloven-hoofed animals, has caused devastating economic losses of global livestock industry[1]. In FMD-endemic areas, the substantial financial burden incurred annually is attributed to the costs of FMD vaccination and the resulting losses of production or culling livestock[2]. The causative agent for FMD is the FMD virus (FMDV), an aphthovirus belonging to the *Picornaviridae* family. It encompasses seven serotypes (O, A, C, Asia 1, SAT 1–3), each with multiple constantly evolving subtypes and no cross-protection between serotypes. Notably, serotype A, which is highly prevalent, demonstrates significant genetic and antigenic heterogeneity within its subtypes[3].

The mature FMD virion (146S) consists of a positive-sense RNA genome enclosed within a pseudo T = 3 icosahedral capsid. The capsid is formed through the assembly of 60 protomers. Each protomer comprises a single copy of the viral capsid proteins VP1, VP2, and VP3, along with an interior VP4 protein. Unlike picornaviruses from other genera, when exposed to mild heating (56 °C) or acidic pH (< 6.5), intact FMDV capsid degrades easily into VP4-deficient pentameric 12S particles and an insoluble aggregate of VP4[4,5].

Inactivated virions serve as the conventional FMD vaccine antigen. The vaccine potency in guinea pigs of 12S particles is 45–400-fold less than that of the intact 146S virion[6]. T-cell responses that aid

[1]State Key Laboratory for Animal Disease Control and Prevention, College of Veterinary Medicine, Lanzhou University, Lanzhou Veterinary Research Institute, Chinese Academy of Agricultural Sciences, Lanzhou, China. [2]CAS Key Laboratory of Infection and Immunity, National Laboratory of Macromolecules, Institute of Biophysics, Chinese Academy of Sciences, Beijing, China. [3]University of Chinese Academy of Sciences, Beijing, China. [4]Wageningen Bioveterinary Research, Wageningen University & Research, Lelystad, The Netherlands. [5]These authors contributed equally: Haozhou Li, Pan Liu, Hu Dong. [6]These authors jointly supervised this work: Huichen Guo, Xiangxi Wang, Shiqi Sun. ✉e-mail: guohuichen@caas.cn; xiangxi@ibp.ac.cn; sunshiqi@caas.cn

neutralizing antibody production also rely on the integrity of 146S[7]. This disparity in immunogenicity contradicts with the conservation of numerous epitopes between 12S and 146S[5,8,9]. The repetitiveness and particle size of viral antigens have also been shown to be the key to eliciting neutralizing antibodies (NAbs) for many viruses, but not for FMDV[10,11]. Thus, although the interaction between FMDV and the host immune system is well studied[12], the molecular basis for the less efficient generation of protective antibodies by 12S is not yet fully understood.

NAbs serve as the primary protective mechanism in animals immunized with FMD vaccines[13,14]. Hence, NAbs and antigenic determinants of FMDV which generate NAbs have raised significant interest. Initial delineation of FMDV antigenic sites primarily involved generating virus escape mutants utilizing NAbs. Studies with NAb escape mutants showed 5 sites where mutations are seen[15]. Others identified 3 mechanisms involved in neutralization[16,17]. Among these mechanisms, there are NAbs targeting the GH loop region of VP1 and thereby interfere with FMDV attachment to the cellular integrin receptor. Another mechanism of NAbs is the binding to VP1 residue 173 (VP1-173), triggering extensive viral aggregation. The third mechanism comprises 146S-specific NAbs, which bind to VP3-175 and VP3-178, they neither impede attachment nor induce aggregation and their underlying neutralizing mechanism remains unresolved. Recently, we isolated 146S-specific single-domain antibodies (VHHs) against serotypes SAT2 and Asia1[18] and serotype A[19] for use in tests to monitor 146S integrity during the vaccine manufacturing process. Others isolated monoclonal antibodies (mAbs) for this purpose[20]. Those studies showed that most antibodies are capable of binding to both 146S and 12S, while antibodies that are specific to either 146S or 12S are more rarely isolated.

In recent years, X-ray crystallography and cryogenic electron microscopy (cryo-EM) studies yielded high-resolution 3D structures of FMDV 146S particles or recombinant virus-like particles (VLPs) for various serotypes and including complexes with integrin receptor or antibodies[21–26]. These studies shed light on the neutralizing mechanism of the FMDV NAbs, which involves simultaneous steric hindrance of integrins and a second cell attachment heparan sulfate receptor, destabilizing the viral capsid[25], or preventing genome release by capsid overstabilization[27]. In contrast to 146S, 12S has only been studied in low resolution (8 Å), and the comparison of the structural differences between 146S and 12S was limited to a mechanistic understanding[5].

In this work, to understand the mechanism underlying the reduced immunogenicity of 12S, we obtain high-resolution cryo-EM structures of FMDV 12S and its immune complex with a VHH binding the interior of the particle, both at a resolution of 3.2 Å, in addition with the resolution of two 146S-specific VHHs complexed to the capsid surface at 3.6 Å and 2.9 Å. To our knowledge, these are the first observations of high-resolution structure of 12S pentamers for any picornavirus, and an antibody targeting the interior of a picornavirus. Furthermore, we conduct comparative studies of the epitope specificity of polyclonal antibodies elicited in pigs either by 146S or 12S particles. By combining these results with available FMDV complex structures, we are able to gain insights into the molecular basis of antigenicity and immunogenicity of different FMDV particle forms.

Results

Characterizations of 146S- and 12S-specific antibodies

In previous studies, we isolated nearly 50 FMDV anti-capsid llama single-domain antibodies[18,19]. Among these, M678F and M688F[19] are 146S-specific for serotype A strain A/TUR/14/98, while M3F is 12S-specific with broad spectrum recognition for all seven serotypes except for SAT2[18] (Fig. 1a). Cell-based neutralization assays indicated that M678F and M688F are neutralizers that both have a 50% neutralizing concentration value (IC_{50}) of 1 μM (95% CI: 0.2–2 μM) (Fig. 1b). Interestingly, a clear synergistic neutralization was achieved by a cocktail of M678F and M688F, with IC_{50} of 0.02 μM (95% CI: 0.01–0.04 μM), indicative of distinct neutralizing mechanisms for these two VHHs. The mixture surpassed the neutralizing potency exhibited by M8 at IC_{50} of 2 μM (Fig. 1b), which was earlier shown to be a potent NAb[25]. Biolayer interferometry (BLI) experiments using strictly monomeric VHHs (suffix K) verified tight interactions for these three antibodies to the antigens with binding affinities (K_D) ranging from 50 to 0.7 nM (Fig. 1e–g). To explore the simultaneous binding of M678F and M688F to 146S capsid, a competitive surface-plasmon resonance (SPR) binding assay was performed. Saturation binding of either M678F or M688F to a sensor loaded with 146S capsid could not prevent the binding of the alternate VHH (Fig. 1c, d). This indicates binding of independent antigenic sites. This underlines the potential of these two antibodies in formulating cooperative two-antibody cocktails as they bind simultaneously to distinct epitopes. As expected based on its 12S specificity, M3F was non-neutralizing, as was earlier shown[28,29].

Structures of 146S FMDV in complex with a two-antibody cocktail

To define the key epitopes and atomic determinants of the interactions between FMDV and its two antibodies precisely, we set out to resolve structures of FMDV mature particles (146S) in complex with M678F or M688F or both M678F and M688F. Icosahedral reconstructions of these three complexes were achieved at resolutions of 3.6 Å, 2.9 Å and 2.9 Å (Supplementary Figs. 1, 2, 3). As expected, M678F and M688F recognize two distinct antigenic sites (Fig. 2a). The density maps show that M678F and M688F target the viral particle around its 3-fold and 5-fold vertices, respectively, and thus up to 60 copies of M678F or M688F could bind to each particle (Fig. 2a–d). In the immune complex with both M678F and M688F, there are a total of 120 antibodies (60 M678F and 60 M688F) concurrently bound to each particle and the interaction modes between M678F/M688F and the particles are essentially indistinguishable to those in 146S-M678F and 146S-M688F complexes. Footprint analysis reveals that 146S-M678F and 146S-M688F extend across two adjacent protomers with a buried area of 913.3 $Å^2$ and 585.7 $Å^2$, respectively on the particle (Fig. 2b, c). All three complementary determining regions (CDRs) of M678F are involved in the engagement with the BC and HI loops from VP3 as well as VP2 HI loop (Fig. 2e and Supplementary Table 1). The 146S-M678F interaction establishes an elaborate hydrogen-bonding network, including 7 hydrogen bonds formed by Y29, D50, S30, R96, R97, and S106 from M678F and K198 and T195 from VP2 and E68, R67, N197 and Q71 from VP3, respectively. The interaction patch in M688F comprises all three CDRs: CDR1 (residue 29), CDR2 (residues 52, 54, and 55), and CDR3 (residues 103 and 114). The epitope recognized by M688F contains 17 residues, only locating in the VP1 BC, CD, EF and HI loops (Fig. 2f). Tight binding between M688F and FMDV is chiefly due to extensive hydrophilic interactions, including 7 hydrogen bonds, the antibody components of these include the side-chains of S29, R52, S54, D55, T103 and Y114, which interact with T87, S173, N43, T45, E83 and D171, respectively (Fig. 2f and Supplementary Table 2).

Double block neutralization mechanisms for a two-antibody cocktail

To shed light on the molecular basis for the synergistic neutralization of FMDV by M678F and M688F, we first explored their effects on the stability of viral particles upon binding at neutral and acidic pH. Particle stability was evaluated by PaSTRy assays[30] to detect exposure to viral RNA. Unlike other NAbs that destabilize/damage viral particles by receptor mimicry, binding of M678F or M688F stabilizes the particles at pH 6.5 by about 4 °C (Fig. 3a). A moderate synergy in increasing viral stability raised by M678F and M688F together, in particular at pH 5.75 was also observed. Given the fact that FMDV uncoating occurs at pH values slightly below neutrality via dissociating into pentamers to

https://doi.org/10.1038/s41467-024-53027-5

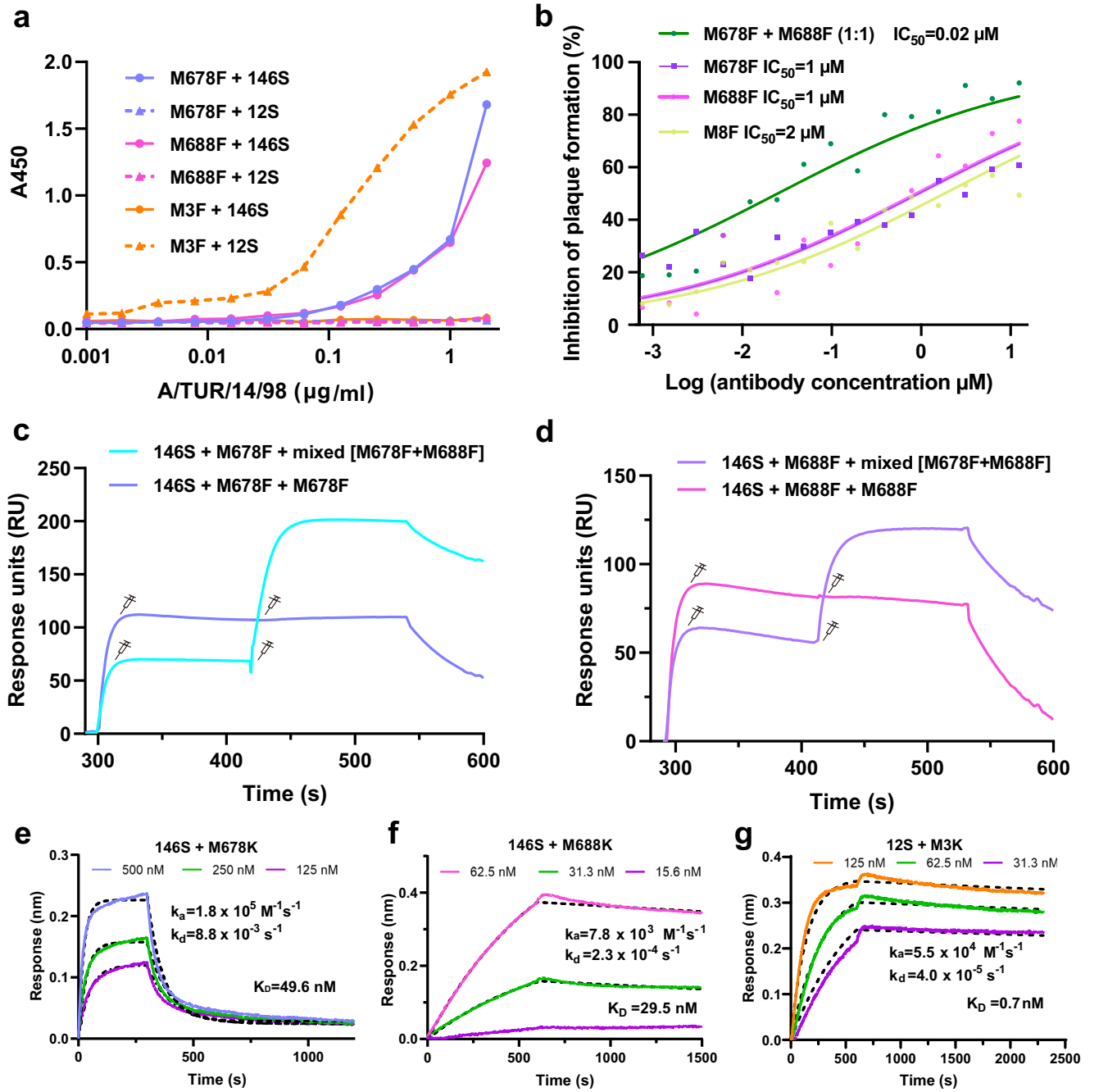

Fig. 1 | Characterization of M678F and M688F. a FMDV particle specificity of M3F, M678F and M688F measured by double antibody sandwich ELISAs. Each plot represents the mean of A450 values from duplicate wells. Source data are provided as a Source Data file. **b** Neutralization of FMDV A/TUR/14/98 by M8F, M678F, M688F and the synergistic neutralization of M678F and M688F using plaque-reduction neutralization assay. Source data are provided as a Source Data file. **c**, **d** Analysis of the simultaneous binding of M678F and M688F to FMDV through a competitive SPR assay. Source data are provided as a Source Data file. **e**–**g** Analysis of FMDV binding affinities of M678K, M688K and M3K by BLI. Sensors loaded with A/TUR/14/98 146S (**e**, **f**) or 12S (**g**) were incubated with concentration series of VHHs at 0 s followed by injection of PBST buffer at 300 s (**e**) or 600 s (**f**, **g**). The BLI response measured at different antibody concentrations (colored curves) was used for global curve fitting according to a 1:1 interaction model. The fitted curves (dotted black lines) were used to derive k_a, k_d and K_D values. Source data of each panel are provided as a Source Data file.

release its genome RNA, physical over-stabilization of viral particles that interfere with normal uncoating may be a possible neutralization mechanism for M678F and M688F. To further verify this speculation, we performed a negative staining EM analysis of these two NAb-virion complexes. Visual inspection of the EM micrographs showed that as many as 95% of FMDV particles incubated with mixture of M678F and M688F were intact at pH 5.75 at room temperature (Fig. 3b). In contrast to this, nearly all unbound FMDV virions had disassembled into pentameric subunits at the same condition (Fig. 3b). Recognition modes of these two antibodies reveal that 60 copies of M678F bind to each particle (Fig. 2a), around the edges of the pentameric building blocks of the virus—specifically, between the 2-fold and 3-fold axes, firmly connecting two neighboring pentamers (Fig. 3c). This binding patch is broadly similar in location to those observed previously for F145 antibody bound to FMDV-OTi and NAb A9 bound to EV71[31]. In general, antibodies specific for epitopes near the 3-fold axis are

https://doi.org/10.1038/s41467-024-53027-5

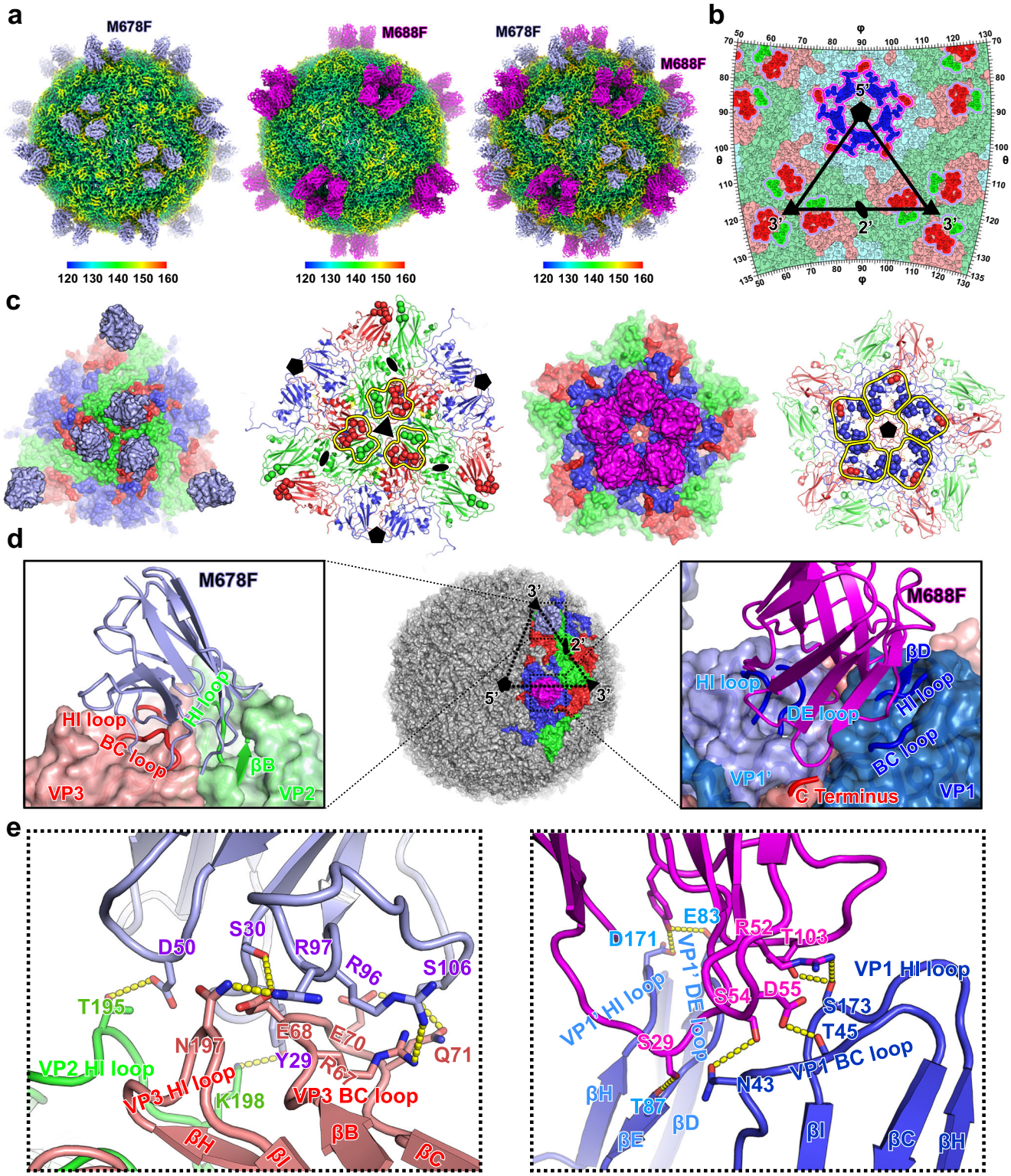

Fig. 2 | Cryo-EM structures of FMDV in complex with M678F or M688F. a Cryo-EM maps of FMDV 146S-M678F-complex (left), FMDV 146S-M688F-complex (middle) and 146S-M678F-M688F complex (right). The FMDV 146S capsids of the complexes are colored by radius scheme as shown by the color bar below; M678F and M688F are colored in lavender and magenta, respectively. **b** Footprints of M678F and M688F on the surface of FMDV 146S. Residues of VP1, VP2, and VP3 are colored in blue, green, and red, respectively. Residues involved in binding to VHHs are outlined in brighter colors corresponding to the protein chain they belong to. The footprints of M678F and M688F are indicated by lavender and magenta lines, respectively. **c** Surface representation (left) and epitopes (right) of M678F and M688F on a pentamer of FMDV 146S. The 146S pentamers are shown as surface (left) or cartoon (right) in the signature colors (VP1, blue; VP2, green; VP3, red), while M678F and M688F are colored in accordance with panel a. The epitopes of M678F (left) and M688F (right) are shown as spheres and those from one epitope are circled by yellow lines. **d** Structural basis of M678F and M688F binding to FMDV 146S. Loops from FMDV 146S involved in interactions with M678F or M688F are shown as ribbon, while the remaining parts are shown as cartoon. M678F and M688F are represented as ribbon. The color scheme is the same as in panel (**a**). **e** Detailed interactions of FMDV 146S with M678F (left), or M688F (right). Residues involved in the binding are shown as sticks and hydrogen bonds are shown as yellow dashed lines.

https://doi.org/10.1038/s41467-024-53027-5

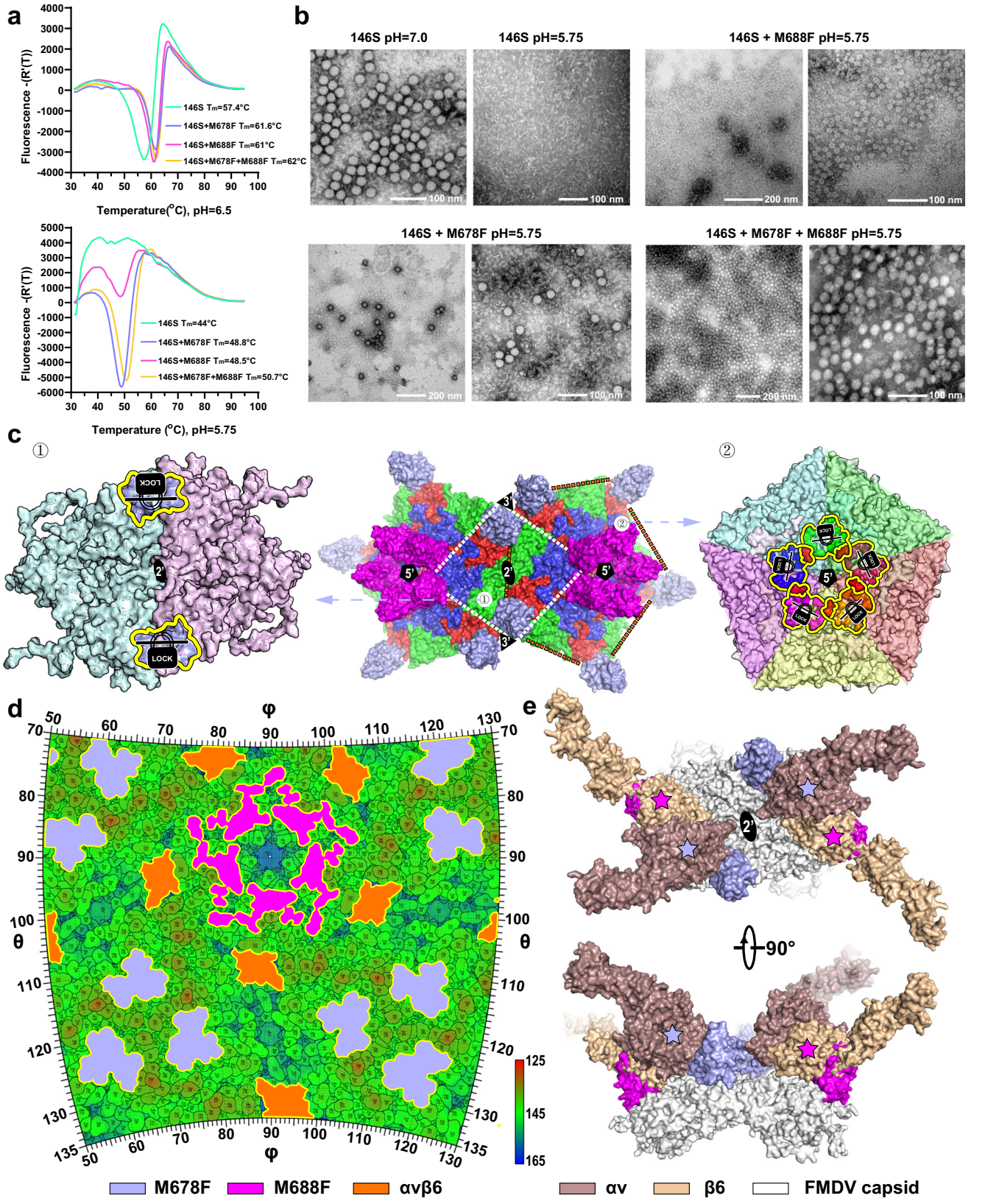

capable of interfering with viral stability and uncoating (e.g., triggering/impeding the conversion from mature virions to uncoating intermediate particles) or even causing physical destabilization/damage to the virions[32]. However, M688F targets to the FMDV outer surface within the pentameric building blocks at a site near the 5-fold axis, stably linking five adjacent VP1 subunits and constructing the "star-shaped" protrusions surrounding the mesa to stabilize the particle (Fig. 3c). These structural evidences support the experimental observation that M678F and M688F synergistically over-stabilize viral particles, subsequently interfering with viral uncoating. FMDV uses integrins as receptors to mediate viral attachment via recognizing a small cleft at the subunit interface of the integrin head[23]. Although the

Fig. 3 | Neutralization mechanism of M678F and M688F. a Thermal stability of FMDV-M678F, FMDV-M688F and synergistic function of FMDV-M678F-M688F complexes determined by thermofluor PaSTRy using SYTO9 dye to detect RNA release. Source data are provided as a Source Data file. **b** Acid stability analysis of FMDV-M678F, FMDV-M688F and FMDV-M678F-M688F complexes using TEM. It was repeated independently once with consistent results. **c** Structural interpretation of antibody stabilization of FMDV. Surface representation of two FMDV pentamers, M678F (light blue) and M688F (magenta) antibodies are displayed in middle of the panel. Two FMDV protomers joined at the 2-fold axis labeled zone 1 (white dotted lines), and a FMDV pentamer labeled zone 2 (orange dotted lines) are zoomed in on the left and right panel, respectively, as indicated by light blue arrows. Epitopes are circled with yellow lines. The axes of rotational symmetry are also marked. **d** Roadmap showing the relative positions of the VHHs (M678F and M688F) and receptors (αvβ6 and HS) footprints on the viral surface. The footprints of M678F, M688F and αvβ6 are outlined with the color bar shown below. **e** Superimpositions of FMDV-αvβ6 and FMDV-M678F/ M688F shown in FMDV 146S zone 1 structure from panel (**d**). The 146S pentamer, M678F, M688F, and receptor subunits αv and β6 are colored as shown by the color bar below. Clashes between M678F/ M688F and receptor subunits are prominent and marked with star symbols.

footprints of M678F and M688F on the FMDV surface do not overlap with the integrins receptor site, superpositions of the FMDV-M678F/ FMDV-M688F and FMDV-αvβ6 complex structures revealed clear clashes between the two subunits of αvβ6 and M678F/M688F (Fig. 3d). Remarkably, the structural overlay analysis reveals that M678F competes with the αv subunit and M688F occupies the β6 subunit binding site (Fig. 3d). Thereby, simultaneous binding of M678F and M688F could synergistically block the attachment of integrin to FMDV owing to the substantially stronger binding affinities of these two antibodies for FMDV when compared to that of the integrin. In summary, M678F and M688F execute their potent neutralization against FMDV infection in a double block mechanism by blocking viral attachment to host cells and interfering with viral uncoating.

High resolution structure of dissociated 12S and altered antigenicity

Native FMDV particles were subjected to low pH treatment, before purifying dissociated 12S pentamers by sucrose density gradient ultracentrifugation (see "Methods"). We determined the first high-resolution structure of 12S pentamers for FMDV at 3.2 Å, and to our knowledge for any picornavirus (Fig. 4a and Supplementary Fig. 3d). The dissociated pentamer is largely ordered, apart from the disorder of VP1 and VP2 N-termini and the loss of VP4, breaking pentamer-pentamer interactions that should have existed in intact capsid. Although the overall structure of dissociated pentamer resembles those in the 146S and 75S particles, dissociated pentamer displays a significantly increased curvature with the top pushing the VP1 external surface more outward and the edge (VP2 and VP3) more inward (Fig. 4b and Supplementary Fig. 3d), presumably due to the lack of geometric restraints raised by the particle formation. In contrast, 146S pentamers are relatively flat, driven by the pentamer-pentamer interactions during the assembly of viral capsid. These structural changes are accompanied by a 3° counterclockwise rotation of the protomeric building block, which pivots about the central shell at the icosahedral 5-fold axis (Fig. 4c). In addition to large-scale disorder (described above), small-scale conformational alterations/shifts primarily occur at the exposed regions, including a number of reported epitopes, such as DE, FG loops of VP1, BC, EF loops of VP2 and EF, HI loops of VP3 (Fig. 4d), indicating likely differences in antigenicity between the 12S and 146S, which is confirmed by several NAbs in this study (Fig. 1). Furthermore, structural details of 12S pentamer also explain our immunogenic results in pigs where the antisera from 12S exhibited ~100-fold lower neutralizing titers against FMDV than those from 146S, albeit both could elicit high and comparable binding antibody titers (Fig. 4e). For many picornaviruses, at least two (mature virions or natural empty particles or uncoating intermediate/dissociated 12S particles) predominate types of particles with various ratios are produced during natural infection[33]. Remarkably, the ratios of these particles that may directly determine immunogenicity and vaccine efficacy could be affected by a number of factors, including viral strain, cell culture conditions, purification procedures and storage conditions. Structural and immunogenic characterizations of 12S pentamers provide lessons for FMDV vaccine production: the procedures for virus production and storage need to be improved to minimize amounts of antigenically altered 12S pentamers, which substantially dilutes protective antigens.

Structural dissections for 12S-specific antibody and NAb category

To further unveil the molecular basis for precise recognitions of 12S- and 146S-specific antibodies, we determined atomic structures of dissociated pentamer in complex with M3F, a 12S-specific non-neutralizing binder (Figs. 5a and 1a). Interestingly, M3F recognizes a conformational epitope located at the inner surface within the edges of the pentamers (Fig. 5a), structurally explaining the incapability in binding to intact viral particles. The binding position for M3F is adjacent to the 3-fold axis, roughly opposite to that observed for M678F, but comparatively more far away from the 3-fold axis. M3F mainly interacts with VP3, involving βD, βE, βF, βG strands and CD, EF, FG loops in VP3 as well as the VP2 N-terminus (Fig. 5b). The epitope for M3F includes residues E52 at the VP2 N-terminus, T104 in VP3 CD loop, H108 in VP3 βD, R120 in VP3 βE, C143 in VP3 EF loop, I144, H145, A146, E147, W148 and D149 in VP3 βF, L152 and N153 in VP3 FG loop, and F156, T157, F158, S159 and P161 in VP3 βG (Fig. 5b and Supplementary Table 3). Extensive hydrophobic interactions contribute to the tight binding between M3F and 12S pentamer (Fig. 5c).

To acquire greater insight as to the antibody binding sites on the FMDV capsid, 12 FMDV NAbs and one 12S-specific binder with available structures[24,25,27], including 3 cryo-EM structures determined in this manuscript (Supplementary Fig. 3 and Supplementary Table 4) were examined. By using cluster analysis on epitope structures, the antibodies were primarily classified into five groups (I, II, III, IV and V) (Fig. 5d). Additionally, we superimposed structures of FMDV capsid from these complex structures and calculated the clash areas between any 2 antibodies (Fig. 5e). Both strategies yielded identical results. Among these, class V antibodies, represented by M3F, are 12S pentamer specific and non-neutralizing. Antibodies from class I and II, target VP1 only around the 5-fold axis, among which class I antibodies form a compact cluster at the "plateau", whereas class II antibodies are more outspread (Fig. 5f). Notably, class II antibodies bind to the VP1 GH loop, directly competing with αvβ6[23,25]. Epitopes for class III and class IV antibodies mainly locate on VP2 and VP3 surrounding the 2- and 3-fold axes, respectively (Fig. 5g). Two further 146S-specific NAbs, M691F and M702F, were earlier shown to bind the same site as M678F and M170, and are thus also class IV NAbs[29]. Remarkably, at least 3 types of NAbs have potential to simultaneously bind to the FMDV capsid, formulating multiple-antibody cocktails to prevent viral infection, akin to polyvalent antiserum elicited by vaccination.

Antibody composition of polyvalent antisera elicited by 12S and 146S particles

Given the fact that 12S and 146S have a different antigenicity, we analyzed antibody composition of polyvalent antisera elicited by equal amounts of 12S or 146S particles in groups of 6 pigs followed for 4 weeks. NAbs emerged one week after vaccination and reached a plateau on 21 days (Fig. 4e). Serum samples on days 28 post

https://doi.org/10.1038/s41467-024-53027-5

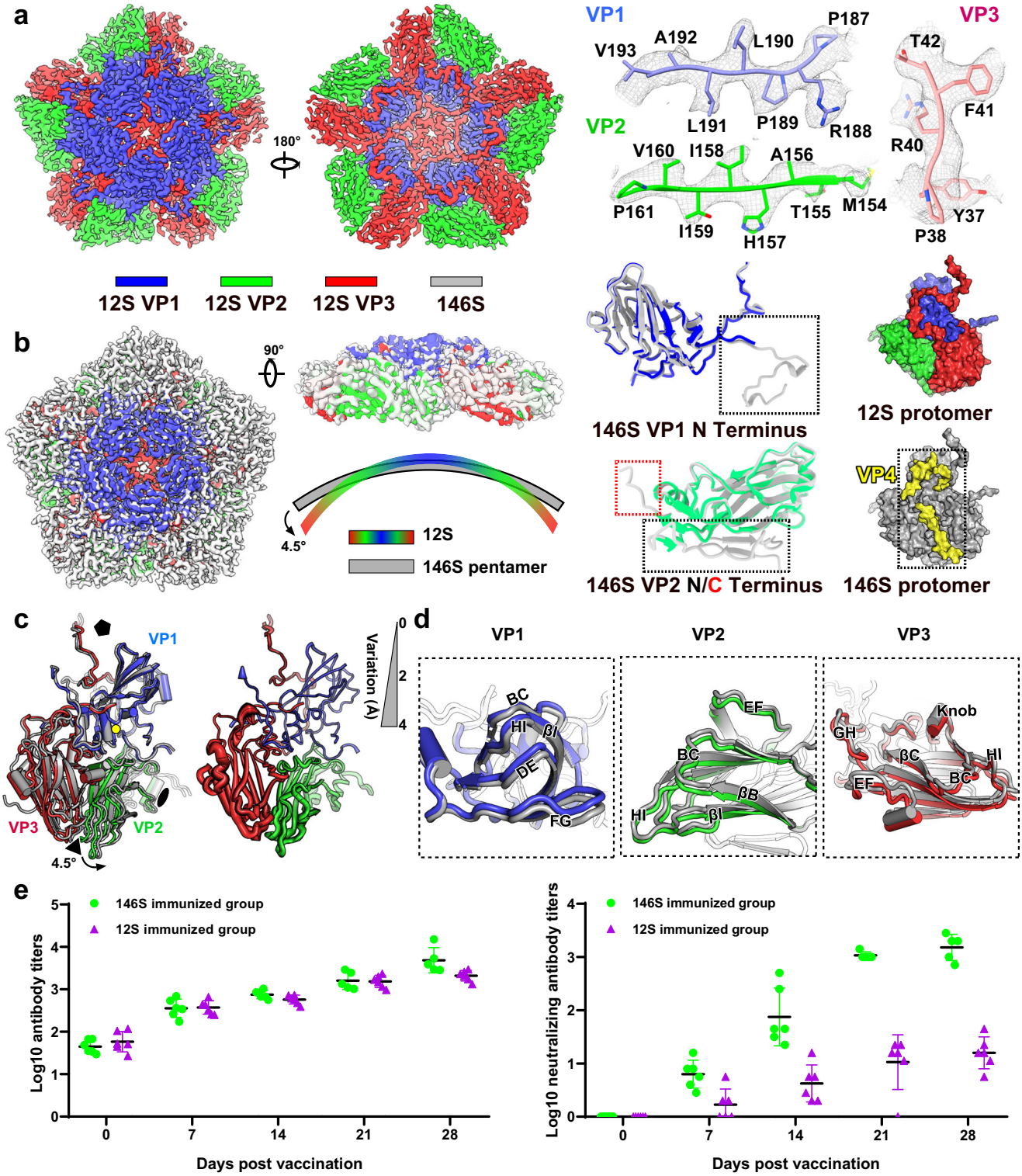

Fig. 4 | Cryo-EM structure of FMDV dissociated pentamer. a Cryo-EM structure of FMDV dissociated pentamer from outside (left) and inside (left middle). The FMDV viral proteins are colored as shown in the legend, while 146S indicates a pentamer that is present in a 146S particle. Electron density maps for C- or N-terminus of VP proteins of the dissociated pentamer (right). **b** Comparison of the structure of a dissociated pentamer (color coded according to panel a) with a superimposed 146S pentamer (white colored) is shown in front view (left), side view (upper right) and cross-section of side view (lower right) on left of the panel. The disordered and thus unresolved N-termini of VP1 and N/C-termini VP2 and the loss of VP4 of dissociated pentamer are displayed on the right. The viral proteins are color coded as panel a. **c**, **d** Structural comparison between 146S and 12S at the protomer level (**c**) and local conformation change within a protomer (**d**). **e** Total FMDV-specific antibody titers (left) and the NAb titers (right) observed after immunizing two groups of pigs with equimolar doses of 146S and 12S at days post vaccination 0, 7, 14, 21, 28. Data are presented as mean values +/- SD of $n = 6$ biologically independent samples for each group are shown. Source data are provided as a Source Data file.

https://doi.org/10.1038/s41467-024-53027-5

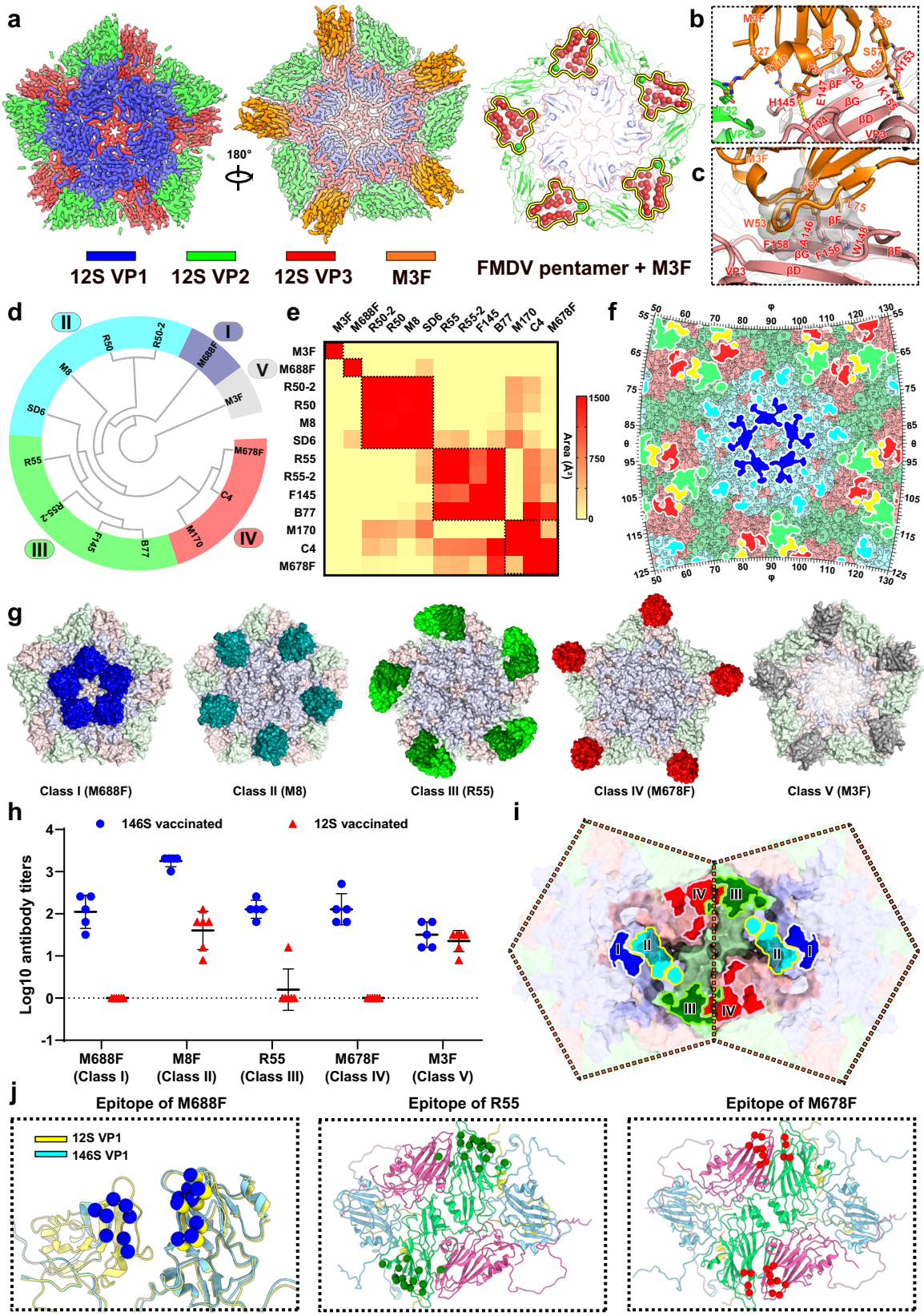

vaccinations were selected and representative antibodies from all five classes were used for liquid-phase blocking ELISA to evaluate their antibody levels in the sera of 146S or 12S immunized pigs. Clearly, antibody titers with similar or competitive epitopes from classes I to IV NAbs were 100-1000-fold higher in 146S immunized antisera than those in 12S vaccinated antisera. By contrary, non-neutralizing Abs using a class V antibody (M3F) were similar between 12S immunized pigs and 146S immunized pigs (Fig. 5h). Antibody composition analysis for polyvalent antisera elicited by 12S and 146S particles dissects the difference in immunogenicity, by which 12S particles are incapable of inducing high levels of various NAbs, but still induce non-neutralizing Abs.

Fig. 5 | Structural topographical classification of FMDV antibodies. a Cryo-EM structure of FMDV dissociated pentamer (12S) complexed with M3F. The complex is displayed from the outside (left) and inside (middle). Independent M3F epitopes (right) are shown as spheres on 12S and circled in yellow. The viral proteins and M3F are colored as indicated in the bar below, consistent across panels. **b**, **c** Detailed interactions between 12S and M3F. Binding residues are shown as sticks, hydrogen bonds as yellow dashed lines, and the hydrophobic pocket in transparent gray. **d** Structure-based antigenic clustering of FMDV antibodies. A total of 13 FMDV antibodies with available structures, including 12 NAbs and M3F that binds the inner capsid, were clustered into five classes (I, II, III, IV, V). **e** Superimposition matrix of FMDV antibody structures' output from epitopes of any two antibodies showing the clustering into five classes. **f** Footprints of the four NAb classes on FMDV 146S are shown, with lighter colors marking each class (as in panel g) and yellow highlighting the overlapping epitopes of class III and IV NAbs. **g** Surface representation model showing five classes of FMDV antibodies bound to 146S or 12S, with classes colored as in panel **d**. **h** A comparison study of serum expression dominance for representatives from each of the five antibody classes between 146S and 12S immunized pig groups. Data are presented as mean +/− SD of $n = 6$ biologically independent samples for each group. Source data are provided as a Source Data file. **i** Footprints of the five antibody classes on adjacent 146S pentamers show specificity for binding at pentamer interfaces or distinct protomers. **j** Epitopes of three 146S-specific NAbs from classes I (left), III (middle), and IV (right), highlighting the molecular basis for 146S specificity. Epitopes are colored by class. Conformational changes between 146S and 12S for class I NAb M688F are shown by superimposing VP1 from 12S onto 146S (left), comparing epitope of M688F (blue dots) with superimposed 12S (yellow dots). Yellow dots are hidden where they overlap with blue. Epitopes of R55 (middle) and M678F (right) span two adjacent protomers across the pentamer interface.

Discussion

The reduced protective efficacy of FMDV dissociated 12S has been observed for decades. However, its molecular mechanism remained elusive due to missing detailed information about alterations at the atomic level. Herein we determined the first high-resolution structure of the dissociated pentamer. Compared to the relatively flat 146S pentamer, the dissociated pentamer possesses a significantly increased curvature, which is accompanied by tectonic shifts, large-scale disorder and conformational shifts at several positions, including the DE, FG loops of VP1, BC, EF loops of VP2 and EF, HI loops of VP3, which affect epitopes of NAbs from classes I, III and IV. Class III NAb R55 and class IV NAb M678F can also exhibit 146S specificity by binding across the interface of two adjacent pentamers at the 3-fold axis, from where 12S dissociates (Fig. 5i, j). In contrast, class I NAb M688F achieves 146S specificity by binding across two adjacent protomers at the 5-fold vertex, where the dissociation leads to increased curvature, enlarging the distance between these protomers at the 5-fold vertex on 12S (Fig. 5j). These structural alterations thus explain the reduced protective efficacy of dissociated pentamers. In addition, we report the structure of the dissociated pentamer complexed to a 12S-specific non-neutralizing VHH (M3F). To our knowledge, it is the first structural observation that an antibody targets the inside of a picornavirus capsid. Surprisingly, the conformational epitope primarily comprises four β-strands in VP3, rather than exposed loops. Even in target animals immunized with 146S, high antibody titers against non-protective epitopes located at the capsid interior were generated as demonstrated by M3F LPBE. These expand our understandings in epitope distributions and antibody response ranging from the outer surface to inner surface and antigenic alterations at atomic resolution.

A high level of capsid flexibility serves as uncoating preparation for picornaviruses. It includes a "breathing" process that involves transient exposure of the N-termini of VP1 and VP4[34], and a pre-dissociation cell entry intermediate[35–37]. In enteroviruses, such intermediates open pores around the 2-fold and quasi-3-fold axes, facilitating the release of the N-termini of VP1, forming a umbilical-like structure connecting the capsid and membrane[38,39], whereas VP4 forms a homo-multimeric virally encoded channel for RNA delivery to the cytoplasm[40]. Belonging to same genus as FMDV, equine rhinitis A virus also exhibits a transient intact empty particle as pre-dissociation cell entry intermediate during the uncoating[41]. Its RNA is also protected from RNases in the endosome[42] and suggested to use same translocation model as enteroviruses[40]. We observed larger disordered regions in the VP1 N-terminus (25 amino acids), VP2 N-terminus (40 amino acids) and C-terminus (7 amino acids) in the 12S comparing to 146S. The disordered regions may provide uncoating cues for FMDV, making the dissociated 12S a byproduct following the uncoating.

Efforts of many investigators over three decades have mapped five functionally independent antigenic sites by neutralization escape mutants[17,43,44]. These sites were only globally defined by identification of critical residues at specific positions. Therefore, a large gap between the observed immune escape and comprehensive epitope distributions at atomic resolution still exists. By using FMDV/antibody complex structures determined in this study as well as previously, we constructed the antigenic landscape with comprehensive epitope distribution, immunogenic and mutational heatmaps on the capsid surface of FMDV (Fig. 5f). Some of the previously identified antigenic sites, indicated by numbers 1 to 5, are related to four classes of antigenic sites assigned in our structural study. Site 1 is mainly linear and trypsin-sensitive, encompassing the GH loop and C-terminus of VP1, which is equivalent to the class II. Sites 2–5 are all conformational and trypsin-resistant except for site 5. Our study did not support the separate classification of sites 1 and 5, which both involve the VP1 GH loop. However, sites 2, 3 and 4 correspond to class III, I and IV, respectively. The classification of sites based on structures also allowed the mapping of a non-neutralizing binder to class V that evidently was not earlier identified by escape mutants. Our classification also allowed analysis of antibody responses against individual epitopes from distinct classes in the serum, and shows divergent antibody lineages were induced by immunization with 146S and 12S.

In previous studies, the therapeutic use of individual antibody and peptide vaccines targeting an individual antigenic site of FMDV demonstrated suboptimal protective efficacy against FMD in target animals[45,46]. As the unique neutralizing epitopes exclusive to 146S facilitate a cooperative humoral defense against FMDV, cocktail therapies targeting these distinctive neutralizing epitopes, along with other NAbs in other classes (Fig. 5d), could be developed for emergency use during FMDV outbreaks to prevent the stamping out of livestock. Antibodies also facilitate opsonization-enhanced phagocytosis, a pivotal process for FMDV clearance in vivo[47]. A recent study further indicates that the in vitro neutralizing potency of antibodies correlates with their opsonophagocytic capability in vivo. NAbs even demonstrate opsonophagocytosis effects at low affinities, highlighting the significance of NAbs in vivo[48].

In conclusion, the antigenic landscape and immunogenic characterizations unveiled in this study will provide guidance for the structure-based rational design of novel highly potent and stable vaccines for protection against FMD.

Methods

Ethics statement

The vaccination study in pigs was approved by the Institutional Review Board of Wageningen Bioveterinary Research (protocol code 2013153). Permissions for pig immunization with FMDV were granted by the Dutch Central Authority for Scientific Procedures on Animals (Project AVD401002015265).

Preparation of 146S particles and 12S particles

FMDV serotype A vaccine strains A/TUR/14/98 and A22/IRQ/24/64 (A22/IRQ) were obtained from the virus production facilities in Lelystad. Briefly, FMDV was amplified in BHK-21 cells grown in suspension in

industrial-scale bioreactors, binary-ethyleneimine inactivated, and concentrated as previously described[19]. FMDV 146S particles were purified by fractionation using 15–45% (w/v) sucrose density gradients (SDG) in Tris-KCl buffer (300 mM KCl; 20 mM Tris.Cl, pH 7.4) for 2 h at 10 °C and 200,000 × *g*. The fractions containing 146S were pooled, concentrated and buffer-changed to PBS or Tris-KCl. The purified 146S content was quantified by absorbance using the extinction coefficient $E_{259\ nm} = 132$[49] and checked for integrity by negative-stain transmission electron microscopy (TEM). SDG-purified A/HuBWH/CHA/2009 146S was provided by the virus production facilities of Lanzhou Veterinary Research Institute. The production and purification process were as for the aforementioned strains. Dissociation of 146S into 12S particles was done by either heating for 1 h at 56 °C or acid treatment, which was done by addition of 1 volume 0.1 M NaH_2PO_4 (pH < 5) to 146S particles, incubation at room temperature for 15 min, and neutralization to pH 7.4 by addition of 1 volume 0.1 M NaOH.

Vaccination of pigs with 146S and 12S antigens

SDG-purified A22/IRQ 146S particles and 12S particles derived thereof by heating were used to compare immunogenicity in pigs. Two double-oil-emulsion vaccines containing either 146S or 12S particles were prepared as described previously[50] using 0.3% BSA and 10% sucrose as excipients to stabilize FMDV particles but lacking the destabilizing excipient thiomersal. Two groups of 6 pigs each were immunized intramuscularly with either 146S or 12S vaccine containing 5 μg 146S or 12S particles per animal. Animal sera were collected on days 0, 7, 14, 21 and 28 post vaccination.

Virus neutralization test

The NAb response was measured by virus neutralization test (VNT) using primary porcine kidney cells following standard procedures[51]. Briefly, two-fold serial dilutions of sera in 96-well plates (50 μl/well) were mixed with 50 μl 100 tissue culture infective doses of A22/IRQ virus required to infect 50% of the wells ($TCID_{50}$) and incubated at 37 °C for 1 h. Then an equal volume of porcine kidney cell suspension was added and plates were placed at 37 °C for 3 days before staining the monoloayers using Amido Black. End point titers were calculated using the Spearmann-Kärber method as the $\log_{10}$ of the reciprocal of the final serum dilution that prevents the cytopathogenic effect in 50% of the wells.

Production of VHHs and antibodies

The VHHs M3, M8[28], M678 and M688[19] were produced in baker's yeast with a C-terminal his6 tag, purified from culture supernatant using immobilized-metal affinity chromatography and biotinylated as previously described[52]. The VHHs M3F, M8F, M678F and M688F (suffix F) were expressed using plasmid pRL188, resulting in additional C-terminal extension with the llama heavy-chain antibody long hinge region, that contains a cysteine for partial disulfide bond formation between two VHHs, and a his6 tag. M3K, M678K and M688K (suffix K) were produced with only a his6 tag using plasmid pUR4584, resulting in strictly monomeric VHHs. Bovine antibody R55 specific for A/HuBWH/CHA/2009 146S particles[27] was kindly provided by dr. Zengjun Lu.

Plaque-reduction neutralization test

FMDV neutralization by VHHs was determined by a plaque-reduction neutralization test (PRNT). VHHs M678F, M688F, M8F or a cocktail of M678F and M688F were 2-fold serially diluted in Dulbecco's Modified Eagle Medium containing 2% fetal bovine serum, with an initial VHH concentration of 2 mg/ml, or 1 mg/ml of each VHH in the cocktail. Two control wells lacking VHHs were included. After adding an equal volume of A/TUR/14/98 virus aiming at 100 plaque-forming units per well and incubation at 37 °C for 1 h, the mixture was transferred to a 6-well culture plate with a monolayer of primary lamb kidney cells. After further incubation for 1 h, the plates were covered with cell medium containing 1% methylcellulose and further incubated till the next day. Then, the overlay was removed, and the cells were stained with Amido Black to visualize plaques. Subsequently, the relative number of plaques in the wells treated with different VHH dilutions as compared to control assays without VHH was calculated. Each assay was performed in duplicate. The VHH concentration required to inhibit 50% (IC_{50}) of the number of plaques was then calculated by four-parameter nonlinear curve fitting using GraphPad Prism 8.0, assuming the same slope for all VHHs and 100% neutralization at a high dose.

FMDV particle stability assay

A thermofluor particle stability thermal release assay (PaSTRy)[30] was performed with a Lightcycler 480 PCR machine in 96-well plates using 1 μg SDG-purified A/TUR/14/98 146S particles in 50 μl 300 mM KCl containing 20 mM phosphate buffer at pH of 5.75 or 6.5. VHHs were added to 146S particles at 5-fold molar excess of VHHs to binding sites (1 μg) to analyze stabilizing effects. The SYTO9 (Thermo Fisher Scientific, Rockford, IL) fluorescent probe with excitation and emission wavelengths of 486 nm and 501 nm, respectively, was added to 5 μM final concentration to detect the single-stranded RNA that is released when virus capsids dissociate. The temperature was ramped from 30 °C to 95 °C in 0.11 °C increments per s. The dissociation of capsids was detected by interpreting the fluorescence signal as the minimum of the negative first-derivative of the fluorescence curve.

Binding affinity measurements

VHH affinity was analyzed by bio-layer interferometry (BLI) using the Octet Red96 System (Sartorius, USA) at 30 °C in PBS containing 0.05% Tween-20 (PBST). High precision streptavidin (SAX)-sensors (Sartorius) were loaded with biotinylated M678F (2 μg/ml) or M8F (1 μg/ml) for 300 s and subsequently with A/TUR/14/98 146S (2 μg/ml) or 12S (1 μg/ml) for 900 s, for subsequent analysis of, respectively, 146S- or 12S-specific binding of unlabeled monomeric (suffix K) VHHs. After a baseline step in PBST for 300 s, the association of serial dilutions of unlabeled VHHs was done for 300–600 s and finally dissociation for 900–1800 s. A reference sensor without unlabeled VHH was included to correct for baseline drift. The on-rate (k_a) and off-rate (k_d) were determined by global fitting of the association and dissociation phases of a series of unlabeled VHH concentrations assuming a 1:1 stoichiometry of VHH binding using Octet Analysis Studio v12.2 software (Sartorius). The equilibrium dissociation constant (K_D), a measure for affinity, was then calculated as the ratio of k_d and k_a.

Surface plasmon resonance competitive assay

To analyze the ability of 2 VHHs to bind simultaneously to FMDV, surface plasmon resonance (SPR) experiments were done using a BIAcore 8 K machine and CM5 sensor chips (Cytiva Life Sciences) in PBST. Unlabeled M678F (399 RU) or M688F (1000 RU) were immobilized individually onto a CM5 sensor chip surface using the EDC/NHS method. SDG-purified A/TUR/14/98 146S of 4 nM was injected onto the chip at a flow rate of 20 μl/min for 120 s. An injection of either 500 nM M678F or 1000 nM M688F was done sufficiently long to ensure complete blocking of antigenic sites, followed by a dual injection of the mixture of 500 nM M678F and 1000 nM M688F. Binding signals were analyzed with BIAevaluation Version 4.1 software.

Negative stain TEM

The effect of VHH binding on acid-induced 146S dissociation was analyzed by TEM. A 5-fold molar excess of VHHs was mixed with FMDV A/TUR/14/98 146S particles in PBS followed by dilution into 20 mM phosphate buffer of pH 5.75 or pH 7.0. After 10 min incubation at room temperature, these samples were deposited onto glow-discharged copper grids for 1 min. After removing the excess sample, the grids were washed twice with PBS and immediately negatively stained for 1 min with 1% phosphotungstic acid (pH 7.0). Excess stain was blotted

away and the grids were loaded into a JEOL 1400Plus Transmission electron microscope for examination.

VHHs binding to FMDV in ELISA

Double antibody sandwich ELISAs using VHHs M3F, M8F, M678F and M688F to detect FMDV particles were done as earlier described[52]. In brief, 96-well polystyrene plates were coated with unlabeled VHH and subsequently incubated with 2-fold serial dilution series of FMDV particles, starting at 2 µg/ml 146S or 12S, in PBST with 1% milk (PBSTM). Bound FMDV particles were detected by subsequent incubation with the biotinylated form of same VHH as used in the coating step, and horse radish peroxidase (HRP)-conjugated streptavidin, followed by staining with 3,3',5,5'-tetramethylbenzidine (TMB). After stopping the staining reaction by the addition of sulfuric acid, the absorbance at 450 nm (A450) was measured. The concentration with 50% binding was assessed using 4-parameter curve fitting.

Liquid phase blocking ELISAs

Pig serum samples from 21 days post vaccination were tested in five liquid phase blocking ELISAs (LPBE) using four different VHHs (M3F, M8F, M678F, M688F) or bovine mAb R55. The LPBEs were performed as described above for the VHH-based sandwich ELISAs, using several modifications that are summarized in Supplementary Table 5. Pig sera were serially 2-fold diluted from 0.9–3.3 log10 for all LPBEs. A 50 µl of diluted serum was mixed with 50 µl of a pre-titrated amount of the antigen. After 16–20 h incubation at 4 °C, 50 µl of these mixtures was transferred to pre-coated plates. After 1 h incubation at room temperature, the plates were washed and incubated with detecting (competing) antibodies. After 1 h incubation, the plates were washed and incubated with conjugates as described above for the VHH-based sandwich ELISAs, while for R55 LPBE, rabbit anti-bovine immunoglobulin–HRP (Sigma Aldrich, St. Louis, MO, USA) was used as conjugate. Control sera of known titers as well as one negative control serum (unvaccinated animal) were included on each ELISA plate as internal standards. Four wells without sera were used as antigen controls (100 % reactivity). Antibody titers were expressed as the logarithm of the reciprocal of the serum dilution giving 50% inhibition of the mean absorbance recorded in the antigen control wells. Serological data were statistically analyzed using two way mixed-effects ANOVA.

ELISAs measuring pig IgG titer

The total pig anti-FMDV IgG titer was determined by an indirect ELISA using plates coated with 1 µg/ml A22/IRQ antigen at 100 µl/well, 4 °C overnight. The antigen consisted of a mixture of 0.5 µg/ml each of 146S and 12S, that was prepared by acidification. The coated ELISA plates were blocked with PBSTM and then incubated with 3-fold dilution series of pig sera starting with a 15-fold dilution. Bound FMDV specific IgG was detected by incubation with a HRP-conjugated polyclonal rabbit anti-pig antibody (Sigma Aldrich), followed by TMB staining and measurement of the A450 as described above. Then, for each serum sample, the absorbance and serum dilution values were fitted to a 4-parameter logistic model and the serum dilution that resulted in an absorbance value equal to twice the background value observed without serum, was interpolated in this curve, using Origin pro 2019[53].

Cryo-EM sample preparation and data collection

Purified M678F and M688F were incubated either individually or as a mixture with purified A/TUR/14/98 146S particles (at a concentration of 0.5 mg/ml) at 4 °C for 1 min at the ratio of ~300 Abs per FMDV 146S particle. A/TUR/14/98 12S particles were prepared by acidification and purified by SDG. In total 3 µl of the purified 12S without antibody or complexed with M3F as well as 146S complexed with M678F, M688F, or the mixture M678F-M688F were applied to a freshly glow-discharged C-flat 1.2/1.3 Au grid (C-flat, CF-2/1-2 C, Protochips). Grids were blotted for 3 s in 100% relative humidity for plunge-freezing (Vitrobot; Thermo Fisher Scientific) in liquid ethane. Cryo-EM datasets were collected at 300 kV using a Titan Krios microscope (Thermo Fisher Scientific) equipped with a K2 detector (Gatan, Pleasanton, CA). Movies (32 frames, each 0.2 s, total dose 60 e − Å−2) were recorded with a defocus of between 1.5 and 2.7 µm using SerialEM, which yields a final pixel size of 1.04 Å.

Image processing, three-dimensional reconstruction, model building and refinement

Data processing was performed using RELION3[54]. Briefly, a total of 3673 micrographs (12S), 5506 micrographs (12S-M3F complex), 2734 micrographs (146S-M678F complex), 501 micrographs (146S-M688F complex) and 2094 micrographs (146S-M678F-M688F complex) first underwent several steps including Motion Correction (MOTIONCORR)[55], CTF Estimation (Gctf)[56], Auto-picking and Particle Extraction from Micrographs. After that, a total of 1,088,637 particles (12S), 2,349,733 particles (12S-M3F complex), 132,191 particles (146S-M678F complex), 53,165 (146S-M688F complex) and 60,791 particles (146S-M678F-M688F complex) were subjected to two-dimensional classification. Finally, 192,654 particles of 12S and 232,071 particles of 12S-M3F complex were used for three-dimensional reconstruction with C5 symmetry imposed, while 46,708 particles of FDMV-M678F complex, 25,824 particles of FMDV-M688F complex and 46,767 particles of FMDV-M678F-M688F complex were used for the icosahedral symmetry reconstruction. The resolution of the final reconstructions was 3.2 Å, 3.2 Å, 3.6 Å, 2.9 Å and 2.9 Å, respectively, as evaluated by Fourier shell correction (threshold = 0.143 criterion). The atomic model of FMDV (PDB code: 7DSS) was initially fitted into the maps with CHIMERA and future corrected, mutated and refined manually by real-space refinement in COOT. The atomic models of M678F, M688F and M3F were built de novo into densities with structures of VHHs as a guide, using COOT. These models were further refined by positional and B-factor refinement in real space with Phenix. Refinement statistics are summarized in Supplementary Table 4.

Antibody clustering

All structures of FMDV complexed with antibodies available in the Protein Data Bank were retrieved and the FMDV protomers were aligned. The buried surface areas between each pair of antibodies were calculated as the inter-antibody distances. Subsequently, a buried surface area matrix clustering was conducted using the pheatmap package in pisa as previously described[57]. Residues on the FMDV protomer within a 4 Å distance from the respective antibodies were identified as epitope residues. The binding frequency of each residue was computed to generate an epitope heatmap. Additionally, a sequence distance matrix clustering was performed using the fitch tool in PHYLIP[58].

Reporting summary

Further information on research design is available in the Nature Portfolio Reporting Summary linked to this article.

Data availability

The cryo-EM density maps of icosahedral reconstructions for 12S, 146S-M678F, 146S-M688F, 146S-M678F + M688F and 12S-M3F have been deposited in the Electron Microscopy Data Bank under accession codes: EMD-34689, EMD-34630, EMD-34636, EMD-34637 and EMD-34690, respectively. The corresponding atomic coordinates have been submitted to the Protein Data Bank with accession numbers: 8HEE, 8HBG, 8HBI, 8HBJ and 8HEG, respectively. Source data are provided with this paper.

References

1. Keeling, M. J. et al. Dynamics of the 2001 UK foot and mouth epidemic: stochastic dispersal in a heterogeneous landscape. *Science* **294**, 813–817 (2001).

2. Knight-Jones, T. J. & Rushton, J. The economic impacts of foot and mouth disease - what are they, how big are they and where do they occur? *Prev. Vet. Med.* **112**, 161–173 (2013).
3. Das, B., Mohapatra, J. K., Pande, V., Subramaniam, S. & Sanyal, A. Evolution of foot-and-mouth disease virus serotype A capsid coding (P1) region on a timescale of three decades in an endemic context. *Infect. Genet. Evol.* **41**, 36–46 (2016).
4. Harmsen, M. M., Jansen, J., Westra, D. F. & Coco-Martin, J. M. Characterization of foot-and-mouth disease virus antigen by surface-enhanced laser desorption ionization-time of flight-mass spectrometry in aqueous and oil-emulsion formulations. *Vaccine* **28**, 3363–3370 (2010).
5. Malik, N. et al. Structures of foot and mouth disease virus pentamers: Insight into capsid dissociation and unexpected pentamer reassociation. *PLoS Pathog.* **13**, e1006607 (2017).
6. Doel, T. R. & Chong, W. K. Comparative immunogenicity of 146S, 75S and 12S particles of foot-and-mouth disease virus. *Arch. Virol.* **73**, 185–191 (1982).
7. Bucafusco, D. et al. Foot-and-mouth disease vaccination induces cross-reactive IFN-γ responses in cattle that are dependent on the integrity of the 140S particles. *Virology* **476**, 11–18 (2015).
8. Cartwright, B., Chapman, W. G. & Brown, F. Serological and immunological relations between the 146S and 12S particles of foot-and-mouth disease virus. *J. Gen. Virol.* **50**, 369–375 (1980).
9. Rao, M. G., Butchaiah, G. & Sen, A. K. Antibody response to 146S particle, 12S protein subunit and isolated VP1 polypeptide of foot-and-mouth disease virus type Asia-1. *Vet. Microbiol.* **39**, 135–143 (1994).
10. Bachmann, M. F. & Zinkernagel, R. M. Neutralizing antiviral B cell responses. *Annu. Rev. Immunol.* **15**, 235–270 (1997).
11. Zolnik, B. S., González-Fernández, A., Sadrieh, N. & Dobrovolskaia, M. A. Nanoparticles and the immune system. *Endocrinology* **151**, 458–465 (2010).
12. McCullough, K. C. et al. Protective immune response against foot-and-mouth disease. *J. Virol.* **66**, 1835–1840 (1992).
13. Pay, T. W. & Hingley, P. J. Correlation of 140S antigen dose with the serum neutralizing antibody response and the level of protection induced in cattle by foot-and-mouth disease vaccines. *Vaccine* **5**, 60–64 (1987).
14. Pay, T. W. & Hingley, P. J. A potency test method for foot and mouth disease vaccine based on the serum neutralizing antibody response produced in cattle. *Vaccine* **10**, 707–713 (1992).
15. Crowther, J. R., Farias, S., Carpenter, W. C. & Samuel, A. R. Identification of a fifth neutralizable site on type O foot-and-mouth disease virus following characterization of single and quintuple monoclonal antibody escape mutants. *J. Gen. Virol.* **74**, 1547–1553 (1993).
16. Baxt, B., Morgan, D. O., Robertson, B. H. & Timpone, C. A. Epitopes on foot-and-mouth disease virus outer capsid protein VP1 involved in neutralization and cell attachment. *J. Virol.* **51**, 298–305 (1984).
17. Baxt, B., Vakharia, V., Moore, D. M., Franke, A. J. & Morgan, D. O. Analysis of neutralizing antigenic sites on the surface of type A12 foot-and-mouth disease virus. *J. Virol.* **63**, 2143–2151 (1989).
18. Harmsen, M. M. et al. Isolation of single-domain antibody fragments that preferentially detect intact (146S) particles of foot-and-mouth disease virus for use in vaccine quality control. *Front. Immunol.* **8**, 960 (2017).
19. Li, H. et al. Novel capsid-specific single-domain antibodies with broad foot-and-mouth disease strain recognition reveal differences in antigenicity of virions, empty capsids, and virus-like particles. *Vaccines* **9**, 620 (2021).
20. Yang, M., Holland, H. & Clavijo, A. Production of monoclonal antibodies against whole virus particles of foot-and-mouth disease virus serotype O and A and their potential use in quantification of intact virus for vaccine manufacture. *Vaccine* **26**, 3377–3382 (2008).
21. Parry, N. et al. Structural and serological evidence for a novel mechanism of antigenic variation in foot-and-mouth disease virus. *Nature* **347**, 569–572 (1990).
22. Kotecha, A. et al. Structure-based energetics of protein interfaces guides foot-and-mouth disease virus vaccine design. *Nat. Struct. Mol. Biol.* **22**, 788–794 (2015).
23. Kotecha, A. et al. Rules of engagement between αvβ6 integrin and foot-and-mouth disease virus. *Nat. Commun.* **8**, 15408 (2017).
24. He, Y. et al. Structures of Foot-and-mouth Disease Virus with neutralizing antibodies derived from recovered natural host reveal a mechanism for cross-serotype neutralization. *PLoS Pathog.* **17**, e1009507 (2021).
25. Dong, H. et al. Structural and molecular basis for foot-and-mouth disease virus neutralization by two potent protective antibodies. *Protein Cell* **13**, 446–453 (2022).
26. Acharya, R. et al. The three-dimensional structure of foot-and-mouth disease virus at 2.9 A resolution. *Nature* **337**, 709–716 (1989).
27. He, Y. et al. Structures of foot-and-mouth disease virus with bovine neutralizing antibodies reveal the determinant of intraserotype cross-neutralization. *J. Virol.* **95**, e0130821 (2021).
28. Harmsen, M. M. et al. Passive immunization of guinea pigs with llama single-domain antibody fragments against foot-and-mouth disease. *Vet. Microbiol.* **120**, 193–206 (2007).
29. Harmsen, M. M., Li, H., Sun, S., van der Poel, W. H. M. & Dekker, A. Mapping of foot-and-mouth disease virus antigenic sites recognized by single-domain antibodies reveals different 146S particle specific sites and particle flexibility. *Front. Vet. Sci.* **9**, 1040802 (2022).
30. Kotecha, A. et al. Application of the thermofluor PaSTRy technique for improving foot-and-mouth disease virus vaccine formulation. *J. Gen. Virol.* **97**, 1557–1565 (2016).
31. Zhu, L. et al. Neutralization mechanisms of two highly potent antibodies against human enterovirus 71. *mBio* **9**, e01013–18 (2018).
32. Wang, K. et al. Serotype specific epitopes identified by neutralizing antibodies underpin immunogenic differences in Enterovirus B. *Nat. Commun.* **11**, 4419 (2020).
33. Jiang, P., Liu, Y., Ma, H. C., Paul, A. V. & Wimmer, E. Picornavirus morphogenesis. *Microbiol. Mol. Biol. Rev.* **78**, 418–437 (2014).
34. Katpally, U., Fu, T. M., Freed, D. C., Casimiro, D. R. & Smith, T. J. Antibodies to the buried N terminus of rhinovirus VP4 exhibit cross-serotypic neutralization. *J. Virol.* **83**, 7040–7048 (2009).
35. Strauss, M., Levy, H. C., Bostina, M., Filman, D. J. & Hogle, J. M. RNA transfer from poliovirus 135S particles across membranes is mediated by long umbilical connectors. *J. Virol.* **87**, 3903–3914 (2013).
36. Xu, L. et al. Atomic structures of Coxsackievirus A6 and its complex with a neutralizing antibody. *Nat. Commun.* **8**, 505 (2017).
37. Baggen, J., Thibaut, H. J., Strating, J. R. P. M. & van Kuppeveld, F. J. M. The life cycle of non-polio enteroviruses and how to target it. *Nat. Rev. Microbiol.* **16**, 368–381 (2018).
38. Ren, J. et al. Picornavirus uncoating intermediate captured in atomic detail. *Nat. Commun.* **4**, 1929 (2013).
39. Shah, P. N. M. et al. Cryo-EM structures reveal two distinct conformational states in a picornavirus cell entry intermediate. *PLoS Pathog.* **16**, e1008920 (2020).
40. Panjwani, A. et al. Capsid protein VP4 of human rhinovirus induces membrane permeability by the formation of a size-selective multimeric pore. *PLoS Pathog.* **10**, e1004294 (2014).
41. Tuthill, T. J. et al. Equine rhinitis A virus and its low pH empty particle: clues towards an aphthovirus entry mechanism? *PLoS Pathog.* **5**, e1000620 (2009).
42. Groppelli, E. et al. Picornavirus RNA is protected from cleavage by ribonuclease during virion uncoating and transfer across cellular and model membranes. *PLoS Pathog.* **13**, e1006197 (2017).
43. Kitson, J. D., McCahon, D. & Belsham, G. J. Sequence analysis of monoclonal antibody resistant mutants of type O foot and mouth

disease virus: evidence for the involvement of the three surface exposed capsid proteins in four antigenic sites. *Virology* **179**, 26–34 (1990).
44. Asfor, A. S. et al. Novel antibody binding determinants on the capsid surface of serotype O foot-and-mouth disease virus. *J. Gen. Virol.* **95**, 1104–1116 (2014).
45. Harmsen, M. M., Fijten, H. P. D., Dekker, A. & Eblé, P. L. Passive immunization of pigs with bispecific llama single-domain antibody fragments against foot-and-mouth disease and porcine immunoglobulin. *Vet. Microbiol.* **132**, 56–64 (2008).
46. Taboga, O. et al. A large-scale evaluation of peptide vaccines against foot-and-mouth disease: lack of solid protection in cattle and isolation of escape mutants. *J. Virol.* **71**, 2606–2614 (1997).
47. McCullough, K. C., Parkinson, D. & Crowther, J. R. Opsonization-enhanced phagocytosis of foot-and-mouth disease virus. *Immunology* **65**, 187–191 (1988).
48. Summerfield, A. et al. Relationship between neutralizing and opsonizing monoclonal antibodies against foot-and-mouth disease virus. *Front Vet. Sci.* **9**, 1033276 (2022).
49. Bachrach, H. L. Foot-and-mouth disease virus: Structure and mechanism of degradation as deduced from absorbance-temperature relationships. *J. Mol. Biol.* **8**, 348–358 (1964).
50. Harmsen, M. M., Fijten, H. P. D., Westra, D. F. & Dekker, A. Stabilizing effects of excipients on dissociation of intact (146S) foot-and-mouth disease virions into 12S particles during storage as oil-emulsion vaccine. *Vaccine* **33**, 2477–2484 (2015).
51. Dekker, A. & Terpstra, C. Prevalence of foot-and-mouth disease antibodies in dairy herds in The Netherlands four years after vaccination. *Res. Vet. Sci.* **61**, 89–91 (1996).
52. Harmsen, M. M., van Hagen-van Setten, M. & Willemsen, P. T. J. Small-scale secretory VHH expression in saccharomyces cerevisiae. *Methods Mol. Biol.* **2446**, 159–179 (2022).
53. Xiang, Y. et al. Simple approach to determine a curve fitting model with a correct weighting function for calibration curves in quantitative ligand binding assays. *Aaps J.* **20**, 45 (2018).
54. Scheres, S. H. RELION: implementation of a Bayesian approach to cryo-EM structure determination. *J. Struct. Biol.* **180**, 519–530 (2012).
55. Scheres, S. H. Processing of structurally heterogeneous Cryo-EM data in RELION. *Methods Enzymol.* **579**, 125–157 (2016).
56. Scheres, S. H. & Chen, S. Prevention of overfitting in cryo-EM structure determination. *Nat. Methods* **9**, 853–854 (2012).
57. Jia, Z. et al. A third dose of inactivated vaccine augments the potency, breadth, and duration of anamnestic responses against SARS-CoV-2. *Protein & Cell*, pwae033. https://doi.org/10.1093/procel/pwae033. (2024) Online ahead of print.
58. Saitou, N. & Nei, M. The neighbor-joining method: a new method for reconstructing phylogenetic trees. *Mol. Biol. Evol.* **4**, 406–425 (1987).

Acknowledgements

We thank Wim van der Poel (Wageningen University) for carefully revising the manuscript, Qianhui Zhu (University of Chinese Academy of Sciences) for help conducting SPR assay, Cynthia Baars and Marga van Hagen-van Setten (Wageningen Bioveterinary Research) for excellent technical assistance. Work was supported by the National Key Research and Development Program of China 2021YFD1800303 to S.S. and H.G., 2018YFA0900801 to X.W., National Natural Science Foundation of China (32072847, 32072859, 32301127) to S.S. and H.G., CAS (YSBR-010) and the National Science Foundation Grants (12034006, 32325004 and T2394482) to X.W., National Science Fund for Distinguished Young Scholar (No. 32325004) and the NSFS Innovative Research Group (No. 81921005) to X.W., Natural Science Foundation of Gansu Province (22JR5RA032, 23JRRA551), Postdoctoral Science Foundation Funded Project (2023M733819, 23JRRA554), Lanzhou Talent Innovation and Entrepreneurship Project(2023-RC-3) to S.S and H.G. The research done at Wageningen Bioveterinary Research was funded by the Ministry of Agriculture, Nature and Food Quality, the Netherlands (project WOT-01-002-034) to A.D.

Author contributions

S.S., X.W., H.G., and M.H. conceptualized and designed the experiments. S.S. and H.G. acquired funding and supervised the project. H.L. and M.H. produced the antibodies. H.L. and D.H. purified the viruses. P.L., D.H., and H.L. performed the structural study. M.H. and A.D. conducted the animal experiment. H.L. conducted all the ELISAs, SPR, and TEM assays. M.H. performed BLI and thermofluor PaSTRy assay. A.D. performed PRNT and VNT assays. H.L. and A.D. conducted the statistics. P.L. and H.L. performed visualization. All authors analyzed data. H.L. and X.W. wrote the manuscript with input from all authors. S.S., M.H., and H.G. reviewed and edited the manuscript.

Competing interests

The authors declare no competing interests.

Additional information

Supplementary information The online version contains supplementary material available at https://doi.org/10.1038/s41467-024-53027-5.

Correspondence and requests for materials should be addressed to Huichen Guo, Xiangxi Wang or Shiqi Sun.

Peer review information *Nature Communications* thanks the anonymous reviewer(s) for their contribution to the peer review of this work. A peer review file is available.